Dynamics of premixed hydrogen/air flames in microchannels

Gianmarco Pizza [a], Christos E. Frouzakis [b,*], John Mantzaras [a],
Ananias G. Tomboulides [c], Konstantinos Boulouchos [b]

[a] *Paul Scherrer Institute, Combustion Research, CH-5232, Villigen PSI, Switzerland*
[b] *Aerothermochemistry and Combustion Systems Laboratory, Swiss Federal Institute of Technology, CH-8092, Zurich, Switzerland*
[c] *Department of Engineering and Management of Energy Resources, University of Western Macedonia, 50100 Kozani, Greece*

Abstract

The stabilization and dynamics of lean ($\varphi = 0.5$) premixed hydrogen/air atmospheric-pressure flames in planar microchannels of prescribed wall temperature are investigated with respect to the inflow velocity and channel height (0.3 to 1.0 mm) using direct numerical simulation with detailed chemistry and transport. Rich dynamics starting from periodic ignition and extinction of the flame and further transitioning to symmetric V-shaped flames, asymmetric flames, oscillating and pulsating flames, and finally again to asymmetric flames are observed as the inlet velocity is increased. The richest behavior is observed for the 1.0-mm-height channel. For narrower channels, some of the dynamics are suppressed. The asymmetric flames, in particular, vanish for channel heights roughly less than twice the laminar flame thickness. Stability maps delineating the regions of the different flame types in the inlet velocity/channel height parameter space are constructed.
© 2007 The Combustion Institute. Published by Elsevier Inc. All rights reserved.

1. Introduction

Combustion at the meso- and microscale has attracted a lot of interest in recent attempts to harness the high specific energy of fuels in miniaturized devices for portable power generation [1]. Progress in the fundamental knowledge of micro- and mesoscale combustion and in the understanding of reactor thermal management is essential for the further development of such systems.

As the combustion volume decreases, several problems appear. Firstly, it becomes more difficult to sustain combustion at small scales because of heat losses and wall termination reactions. Recent studies have demonstrated the feasibility of stable combustion inside burners with dimensions even smaller than the classical flame quenching distance. One such example is the Swiss roll burner, which is based on excess enthalpy combustion [2]; therein flame sta-

* Corresponding author. Fax: +41 44 632 1255.
 E-mail address: frouzakis@lav.mavt.ethz.ch
(C.E. Frouzakis).

bilization is accomplished by preheating the feed by means of burnt gas heat recirculation. Miesse et al. [3] demonstrated the stabilization of homogeneous (gasphase) methane/oxygen diffusion flames between parallel plates having gaps less than 1 mm. This was accomplished by special treatment of the reactor wall surfaces rendering them "quenchless," i.e., inactive with respect to the recombination of gas phase radicals. Thus, a flame can be established in narrow channels either by increasing the wall temperature, e.g., excess enthalpy combustion, or by appropriately treating the wall surface, e.g., the "quenchless" surface.

Another problem that arises in reduced-size combustors is the strong flame–wall interaction, which dramatically changes the characteristics of flame propagation. Maruta et al. [4] have studied experimentally the combustion of methane–air mixtures in quartz glass microtubes 2.0 mm in diameter (slightly smaller than the quenching distance), and of either straight or U-shaped configuration, at a fixed wall temperature. For different combinations of the equivalence ratio and the inflow velocity, they observed three different regions—flame oscillations, stable flame, and no flame. Flame oscillations along the channel axis were observed at low inflow velocities and equivalence ratios close to the stoichiometric value. This was interpreted as a repetitive, periodic process of flame ignition and extinction. The characteristics of methane/air and propane/air premixed flames in straight cylindrical quartz tubes, 2 mm in inner diameter, with a wall temperature profile controlled by an external heat source, were analyzed experimentally and numerically by Maruta et al. [5]. In addition to the three aforementioned combustion modes, they reported other flame types with rich dynamics. Those included a 1-D pulsating flame, moving periodically along the channel axis in a regular fashion, and a second type combining the characteristics of the pulsating and the extinction–ignition periodic flame. Richecoeur and Kyritsis [6] observed a repetitive-periodic extinction–ignition in nonpremixed methane/oxygen combustion inside a curved mesoscale duct of internal diameter 4.0 mm. They reported an increase of frequency with decreasing tube diameter. Miesse et al. [3] have shown that the diffusion flame in their submillimeter combustor had a structure different from that expected in a similar burner configuration at a macroscopic scale. They observed some unique isolated reaction zone structures, similar to cellular instabilities.

The aforementioned studies indicate that new flame dynamics and structures appear in micro- or mesoscale combustion. Premixed flames exhibit two intrinsic instability mechanisms associated with their propagation: hydrodynamic instability and diffusive–

thermal instability. The hydrodynamic instability, discovered by Darrieus and Landau (the DL instability) [7,8], originates from the density jump across the flame front. In the review work of Bychkov and Liberman [9], it is reported that for realistic heat expansion coefficients, only a planar flame can propagate in a narrow tube with height smaller than half of a characteristic cutoff wavelength (determined from the DL theory for unity Lewis number and a single-step high activation energy reaction) because of thermal stabilization effects. The calculated value of the cutoff wavelength for realistic flames is about two orders of magnitude larger than the flame thickness, suggesting that for micro- or mesoscale applications this type of instability should not be present. The thermal–diffusive instability, first investigated in [10,11], is induced by the imbalance between mass and thermal diffusion of the combustion mixture and it appears at sufficiently low/high values of the Lewis number of the deficient reactant. There are two types of thermal–diffusive instabilities: cellular instability [12] for Lewis numbers smaller than unity by less than a critical value and pulsating instability for Lewis numbers exceeding a critical value that is larger than unity [13,14].

The present work investigates H_2/air atmospheric-pressure combustion in a plane 2-D channel configuration. Hydrogen has attracted increased attention in recent years as a fuel because it allows CO_2- and soot-free combustion. Hydrogen-enriched combustion of hydrocarbon fuels is also considered in many practical systems such as gas turbines and automotive engines.

For microscale fuel-lean hydrogen/air combustion, only thermal–diffusive cellular instability is expected, since the Lewis number of the limiting reactant is less than unity. The strong flame stretch at the small scales has a stabilizing effect [15], whereas the heat losses are destabilizing [16] and can further induce oscillations in nearly unity-Lewis-number flames similar to those encountered in large-Lewis-number flames [17]. Therefore, the particular characteristics of fuel-lean hydrogen/air combustion in nonadiabatic meso-/microscale 2-D channels cannot be inferred from simple theoretical considerations.

Up to now, there have been no detailed experiments in microscale combustion systems, mainly because of the difficulty of carrying out spatially resolved measurements at small scales. Therefore, detailed mathematical modeling is indispensable in understanding the combustion dynamics and in assisting the design of such systems. To this direction, a number of investigations have been reported in the literature. The thermodiffusive approximation is commonly employed to bypass the solution of the Navier–Stokes equations. Using single-step chemistry, Daou

and Matalon [18] studied the influence of the ratio of the channel height to the flame thickness and the ratio of the flow velocity to the laminar flame speed on the propagation of a flame subject to a prescribed Poiseuille flow in an adiabatic channel. Using single-step chemistry, Jackson et al. [19] qualitatively captured experimental observations in narrow circular tubes [6] within the thermodiffusive approximation.

In other recent works, the coupling of flow and chemistry is taken into account, but other simplifying assumptions are made. Raimondeau et al. [20] simulated stoichiometric methane/air combustion in a microchannel using a 2-D steady parabolic (no axial diffusion considered) model with detailed chemistry/transport and symmetry boundary conditions on the tube axis. They obtained stable flames for radii ranging from 0.1 to 10 mm. Kim and Maruta [21] simulated a premixed methane/air flame in circular tubes with diameters ranging from 0.4 to 4.0 mm for different combinations of thermal (adiabatic or isothermal) and velocity boundary conditions. Using a steady formulation and a single-step irreversible reaction, they analyzed the flame shape, the propagation velocity, and the flow velocity variations generated by the flames. Norton and Vlachos [22] simulated premixed methane/air mixtures in a microchannel consisting of two 1-cm-long infinitely wide plates placed at a distance of 0.4 to 4.0 mm apart. They used single-step chemistry and symmetry boundary conditions at the midplane. The authors analyzed the effects of microburner dimensions, materials of construction, external heat loss, and inflow velocity on flame stability and combustion characteristics, using steady simulations for the bulk of their results. Unsteady behavior was also examined; under certain conditions and for low inflow velocities a combustion mode characterized by periodic ignition/extinction similar to the experimental observations of Maruta et al. [4] was reported. In a subsequent study, Norton and Vlachos [23] repeated their 2-D steady computations for propane/air mixtures. A wider range of stable operating conditions was observed in propane/air flames compared to methane/air flames. More recently, Karagiannidis et al. [24] investigated the stability of methane/air mixtures in catalytic microchannels using a 2-D steady model with detailed hetero-/homogeneous reaction schemes; it was shown that when gas-phase chemistry was added to the heterogeneous chemistry, the stability limits of catalytic microreactors were extended.

From the works reported above, it appears that combustion at the micro-/mesoscale has some peculiarities. This problem has not yet been analyzed in appropriate detail. In fact, all the referenced numerical investigations employ at least one of the following simplifying assumptions: single-step chemistry, steady formulation, symmetry condition at the symmetry plane for 2-D channels or axisymmetric modeling in cylindrical channels (which precludes the formation of asymmetric flames), or thermodiffusive approximation. These simplifications can potentially have a strong effect on the observed combustion dynamics.

The flame dynamics in microchannels depend on a number of parameters: the geometric properties of the channel (height and length-to-height ratio), the inflow mixture properties (inflow velocity profile, mixture composition and temperature), and the wall boundary conditions that affect the transfer of heat (fixed-temperature, adiabatic, or conducting walls) and mass (nonreactive walls, walls where gas-phase radicals can recombine, or catalytic walls) to or away from the solid surfaces.

The present work undertakes a systematic numerical investigation of fuel-lean (equivalence ratio, $\varphi = 0.5$) hydrogen/air combustion dynamics in microscale plane channels. A transient fully elliptic code is used to simulate the flame–flow coupling in the entire channel (i.e., without imposing symmetry at the midplane), taking into account the detailed description of chemistry and transport. The goal is to map the flame dynamics as a function of two parameters: the inflow velocity, U_{IN}, which is assumed to be uniform, and the channel height, h. The inflow velocity is varied between 4 and 400 cm/s, while the channel height ranges between 0.3 and 1.0 mm. The other defining parameters are kept fixed.

2. Computational approach

The geometry consists of a channel between two parallel, infinitely wide plates, with a fixed length-to-height aspect ratio $L/h = 10$.

2.1. Governing equations

The governing equations are those for 2-D continuity, momentum, energy, and chemical species at the low-Mach-number limit for open systems [26], together with the equation of state (ideal gas law):

Continuity:

$$\frac{\partial \rho}{\partial t} + \nabla \cdot (\rho \underline{u}) = 0. \tag{1}$$

Momentum:

$$\rho \left(\frac{\partial \underline{u}}{\partial t} + \underline{u} \cdot \nabla \underline{u} \right) = -\nabla p_1 + \nabla \cdot (\mu \underline{\underline{S}}), \tag{2}$$

$$\underline{\underline{S}} = \nabla \underline{u} + (\nabla \underline{u})^T - \frac{2}{3} (\nabla \cdot \underline{u}) \underline{\underline{I}}. \tag{3}$$

Energy:

$$\rho c_{\mathrm{p}} \left(\frac{\partial T}{\partial t} + \underline{u} \cdot \nabla T \right)$$

$$= \nabla \cdot (\lambda \nabla T) + \sum_{i=1}^{N} h_i \dot{\omega}_i$$

$$- \rho \left(\sum_{i=1}^{N} c_{\mathrm{p},i} Y_i \underline{V}_i \right) \cdot \nabla T, \tag{4}$$

$$c_{\mathrm{p}} = \sum_{i=1}^{N} c_{\mathrm{p},i} Y_i. \tag{5}$$

Species:

$$\rho \left(\frac{\partial Y_i}{\partial t} + \underline{u} \cdot \nabla Y_i \right) = -\nabla \cdot (\rho Y_i \underline{V}_i) + \dot{\omega}_i,$$

$$i = 1, \ldots, N. \tag{6}$$

Ideal gas law:

$$p_0 = \rho R T. \tag{7}$$

In the low-Mach-number formulation, Eq. (1) is replaced by Eq. (8) below, which is obtained by combining the continuity (1), energy (4), species (5), and state equations (7):

$$\nabla \cdot \underline{u} = -\frac{1}{\rho} \left(\frac{\partial \rho}{\partial t} + \underline{u} \cdot \nabla \rho \right)$$

$$= \frac{1}{\rho} \sum_{i=1}^{N} \frac{\overline{W}}{W_i} (-\nabla \cdot \rho Y_i \underline{V}_i + \dot{\omega}_i)$$

$$+ \frac{1}{\rho c_p T} \left[\nabla \cdot (\lambda \nabla T) - \sum_{i=1}^{N} h_i \dot{\omega}_i \right.$$

$$\left. - \rho \left(\sum_{i=1}^{N} c_{p,i} Y_i \underline{V}_i \right) \cdot \nabla T \right]. \tag{8}$$

In Eqs. (1) to (8), λ is the thermal conductivity, h_i and $\dot{\omega}_i$ are the enthalpy and chemical production term for species i, Y_i and $\underline{V}_i$ are the mass fraction and diffusion velocity of species i, p_1 and p_0 are the hydrodynamic and the thermodynamic pressures, W_i and $\overline{W}$ are the molecular weight of the ith species and the mean molecular weight, and $c_{\mathrm{p},i}$ and c_p are the ith species and mixture heat capacities, respectively. $\underline{\underline{I}}$ is the identity matrix, while the species diffusion velocities $\underline{V}_i$ are

$$\underline{V}_i = -(D_i/X_i)\nabla X_i, \tag{9}$$

with D_i the ith species mixture-averaged diffusivity.

2.2. Boundary conditions and solution method

At the channel inlet, uniform profile for the inlet velocity (U_{IN}), flux boundary conditions for the incoming species mass fractions, and constant temperature ($T_{\mathrm{IN}} = 300$ K) are applied. Along the channel walls, a fixed temperature profile is imposed: it ramps smoothly, via a hyperbolic tangent function, from the temperature of the cold inflow mixture, $T_{\mathrm{IN}} = 300$ K, to the wall temperature, $T_{\mathrm{W}} = 960$ K, over the initial 1/20 channel length. The prescribed wall temperature is a typical boundary condition in both experiments and simulations [4,5]. The maximum wall temperature of 960 K was chosen so as to establish flames inside the channel at realistic inflow velocities. Zero flux for all species and no-slip boundary conditions are employed for the velocity at the gas–wall interfaces. In this respect, radical wall recombination reactions are not considered. Finally, Neumann boundary conditions are imposed at the right end of the computational domain, and buoyancy is neglected.

The parallel numerical approach that solves the system of Eqs. (1)–(8) is based upon the spectral element method for spatial discretization. The computational domain is split into a number of quadrilateral elements and the data and geometry are expressed as sums of high-order tensor product polynomials [25]. A high-order splitting scheme for low-Mach-number reactive flows that separates the thermochemistry (species and energy) from the hydrodynamic (continuity and momentum) subsystems is used for time integration [26]. The integration of thermochemistry is performed with the matrix-free, fully implicit, parallel stiff ODE solver PVODE [27]. Details on the mathematical formulation, the numerical method, as well as validation of the approach with asymptotic analysis and numerical benchmark tests can also be found in [26].

The gas-phase chemistry is described by the mechanism of Yetter et al. [28]. Mixture-average transport is used, based on the CHEMKIN transport database [29], while the chemical reaction rates are evaluated with CHEMKIN [30].

2.3. Computational domain

The 2-D domain was discretized with eight spectral elements in the transverse direction and 60 elements in the streamwise direction, all equally spaced. To determine the grid requirements, the thermal flame thickness is firstly evaluated according to [31],

$$L_{\mathrm{f}} = \frac{T_{\mathrm{f}} - T_{\mathrm{IN}}}{\max \left| \frac{\partial T}{\partial x} \right|}, \tag{10}$$

where T_{IN} and T_{f} are the temperatures of the unburned and burned mixture, respectively, and

$\max\left|\frac{\partial T}{\partial x}\right|$ is the maximum temperature gradient along the flame coordinate. The temperature and species profiles of a lean premixed laminar H_2/air flame ($\varphi = 0.5$) with an inlet temperature $T_{IN} = 300$ K were computed using the PREMIX code of CHEMKIN [32]. For the conditions considered, the resulting flame thickness is $L_f = 0.39$ mm, the laminar flame speed is $S_L = 58$ cm/s, and the adiabatic flame temperature is $T_f = 1630$ K. The same grid was used for all channels with heights ranging from 0.3 to 1.0 mm. Therefore, a resolution analysis is presented below only for the larger channel height ($h = 1.0$ mm), since the resolution requirements for narrower channels are less strict.

Using sixth-order Legendre–Lagrangian interpolating polynomials per direction and element, a total of 361 grid points are employed in the streamwise direction, corresponding to an average spatial resolution of $\Delta x = 0.028$ mm and resulting in approximately $L_f/\Delta x = 14$ grid points within the flame zone. The solution was not significantly affected when the polynomial order was increased to 8 and subsequently to 10, corresponding to 19 and 23 points inside the flame, respectively, confirming the grid-independence of the solution. Since the grid is even finer in the transverse direction, no further tests were performed for the resolution in that direction. Simulations were carried out on a Linux cluster. On two CPUs running with a clockspeed of 2.4 GHz, and depending on the initial condition, a typical calculation for a complete simulation from the initial condition to the final state (steady or oscillatory) with a grid consisting of a total of 16,920 discretization points required between 15 and 40 h.

3. Results and discussion

3.1. Description of the ignition process

The emphasis of the present work is on the dynamic behavior observed after a stable flame is established in the numerical domain rather than on the ignition process itself. Therefore, a typical ignition process is described here only qualitatively. The initial conditions for ignition consisted of a channel filled with a cold mixture having the same composition, temperature, and velocity as the inflow mixture. Heat transfer from the hot walls generates HO_2 radicals at the wall vicinity, followed first by a radical runaway process, typical of low-temperature hydrogen ignition, and, subsequently, by thermal runaway. For cases where the incoming flow velocity is higher than a critical value, radicals are convected away from the walls and out of the domain faster than they are

produced, and the initial radical buildup does not result in the establishment of a stable flame inside the computational domain.

3.2. Dynamic behavior for the 1.0-mm-height channel

The simulated velocity range corresponds to incoming Reynolds numbers (based on the channel height h, the inflow velocity U_{IN}, and the mixture kinematic viscosity $\nu = 0.1887$ cm^2/s) in the range $2.1 \leqslant Re_{IN} \leqslant 212$. Four different flame types are observed as the inlet velocity is increased: periodic extinction/ignition, V-shaped flames, asymmetric and oscillating flames.

3.2.1. Periodic ignition and extinction ($4 \leqslant U_{IN} \leqslant 18$ cm/s)

For the lowest inflow velocities considered, $4 \leqslant U_{IN} \leqslant 18$ cm/s, a periodic sequence of flame ignition and extinction is observed. The cold mixture entering the channel is heated up by the hot walls, ignites at a certain downstream location, and then propagates back toward the inflow consuming all the fuel along its way. As the flame reaches the cold inflow region it extinguishes due to heat losses, and the fuel starts to fill the entry section again until it reignites; the whole process repeats itself periodically with a constant frequency that depends on the inflow velocity. During the ignition phase, the mixture is heated up and moves from the low-temperature branch of the S-shaped ignition diagram to the vigorously burning branch. After ignition, the fuel is completely consumed, and the system, after crossing the extinction point, returns to the low temperature branch. The whole cycle then starts again.

Fig. 1a depicts the temporal variation of the maximum temperature inside the channel for $U_{IN} = 10$ cm/s; this parameter changes periodically at a frequency of 106.9 Hz between the wall temperature, $T_W = 960$ K, and the maximum flame temperature, 1578 K, with long periods of relative inactivity (associated with the flow of fresh mixture into the channel and the buildup of a radical pool) followed by sudden bursts (associated with radical and eventually thermal runaway and subsequent fast flame propagation). For all extinction/ignition cases, the flame has a symmetric shape and the maxima of all intermediate species and temperature are located on the midplane ($y/h = 0.5$). For the conditions considered here, the nonburning solution is unstable. The observed limit cycle ignition/extinction behavior has resulted from the loss of stability of this nonburning solution via a Hopf bifurcation.

The temporal evolution of the flame location, defined as the streamwise position of the maximum
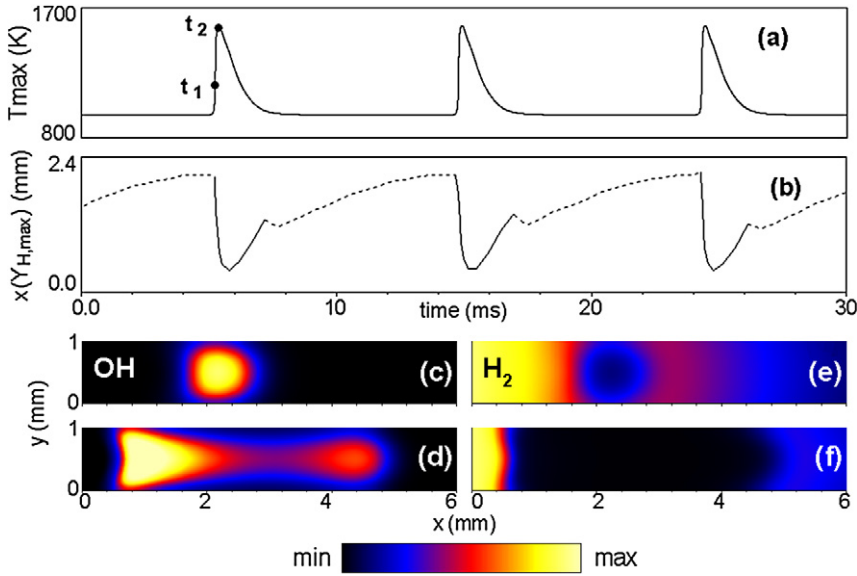
Fig. 1. Ignition/extinction behavior in the $h = 1.0$ mm height channel at $U_{IN} = 10$ cm/s: (a) temporal variation of the maximum temperature inside the channel, (b) streamwise location of the maximum H mass fraction (the solid line corresponds to $Y_{H,max} > 10^{-7}$—burning flame—and the dotted one to $Y_{H,max} < 10^{-7}$—no flame), (c, d) 2-D maps of the OH mass fraction, and (e, f) 2-D maps of the H_2 mass fraction. The maps in (c, e) and (d, f) correspond to the time instants t_1 (= 5.69 ms) and t_2 (= 5.83 ms), respectively, shown in (a). The minimum in the color-coded bar corresponds to zero and the maximum to 3.2×10^{-3} for OH and 1.2×10^{-2} for H_2, respectively. For clarity, only the first 6 mm of the channel are shown.

H mass fraction, $x(Y_{H,max})$ along the midplane is shown in Fig. 1b. The solid line marks the ignition process (i.e., the time intervals when $Y_{H,max} > 10^{-7}$), while the dashed line corresponds to the time intervals during which $Y_{H,max} < 10^{-7}$, i.e., the time during which the radical pool is formed. Ignition occurs at $x(Y_{H,max}) \approx 2.1h = 2.1$ mm and the flame propagates upstream as close as ∼0.4 mm away from the inflow.

In Figs. 1c and 1e the contours of the OH and H_2 mass fractions at a time instant shortly after ignition (marked with t_1 in Fig. 1a) are presented. The flame is nearly hemispherical at the beginning; it then expands outward and propagates both in the upstream and the downstream direction, Figs. 1d and 1f. The upstream propagating front extinguishes when it reaches the cold inflow, while the downstream propagating one does so when the local H_2 concentration drops below the flammability limit (Figs. 1d and 1f). It is interesting to observe that the upstream propagating flame changes curvature during propagation, exhibiting first a convex (Fig. 1c) and finally a concave (Fig. 1d) shape toward the unburned mixture; the downstream propagating front maintains the initial convex shape toward the unburned mixture [18,33]. The velocity of the upstream propagation, obtained from the time derivative of the flame location, reaches its maximum value of around 15 m/s shortly after ignition.

This flame behavior persists for inlet velocities ranging from 4 to 18 cm/s; both the amplitude and the frequency of the temperature oscillations inside the channel increase with increasing inlet velocity (Fig. 2). Similar behavior has been reported elsewhere. Maruta et al. [5] have experimentally studied CH_4/air flames at equivalence ratio $\varphi = 0.5$ in tubes of internal diameter 2.0 mm. For a fixed average mixture inlet velocity of 30 cm/s, repetitive extinction and ignition with a frequency of 50 Hz was observed at their lowest maximum heated-wall temperature (1130 K). Near extinction, Norton and Vlachos [22] also observed similar oscillatory behavior in their CFD calculations of CH_4 flames in a channel with a height of 0.6 mm. In the cases of high heat loss, a limit-cycle behavior with a period of about 1 ms was reported.

3.2.2. V-shaped stable flame ($8 \leqslant U_{IN} \leqslant 75.5$ cm/s)

As the inlet velocity is increased, the flame is progressively restricted from propagating toward the inflow. Eventually, the oscillatory behavior ceases, and a V-shaped stable symmetric flame is established for a critical value of U_{IN} between 18 and 19 cm/s. This flame type persists for inflow velocities up to $U_{IN} = 75.5$ cm/s, stabilizing farther away from the inlet as U_{IN} increases.

For $U_{IN} < 70$ cm/s, the maximum temperature and maximum concentration of all radicals are located
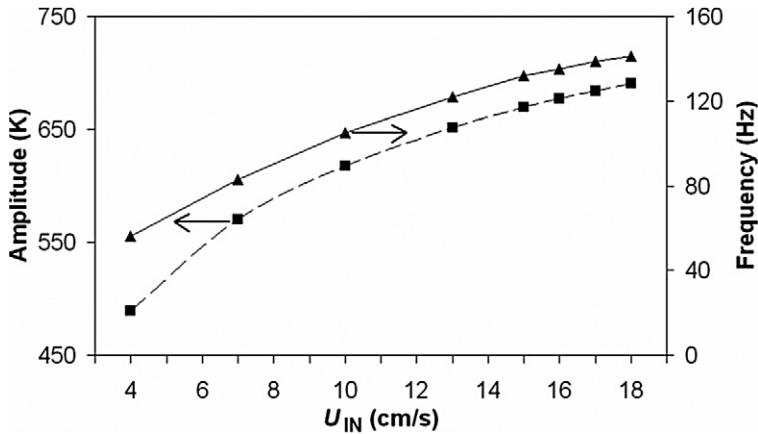
Fig. 2. Amplitude ($T_{\max} - T_{W}$) and frequency of the temperature oscillations inside the $h = 1.0$ mm channel as a function of the inlet velocity over which ignition/extinction behavior is observed.
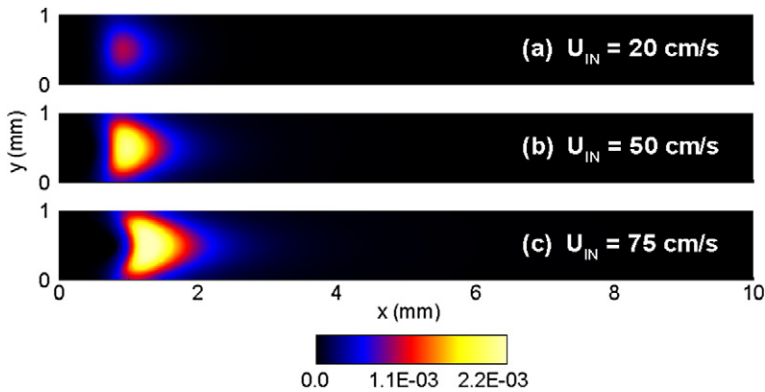

Fig. 3. V-shaped type flames in the $h = 1.0$ mm height channel: OH radical mass fraction at various inlet velocities: (a) $U_{IN} = 20$ cm/s, (b) $U_{IN} = 50$ cm/s, and (c) $U_{IN} = 75$ cm/s.

on the midplane ($y/h = 0.5$), as shown in Fig. 3 for Y_{OH}. For $U_{IN} > 70$ cm/s, a change is evident in the internal flame structure (Fig. 4a for $U_{IN} = 75$ cm/s): the flame is still V-shaped and stable with the maximum of the temperature and mass fractions of all radicals, except H, located on the midplane. The distribution of Y_H, however, differs markedly: it remains overall symmetric around the midplane, but two maxima are formed slightly off the midplane and symmetric with respect to it.

It is also worth pointing out that as U_{IN} is varied within the range of stability of V-shaped flames, the steady state is approached in a damped oscillatory manner; i.e., the V-shaped flame overshoots the final stabilization location, pulsates around it with decreasing amplitude, and eventually stabilizes.

Starting with the stable V-shaped flame for $U_{IN} = 18$ cm/s, and decreasing the inlet velocity in steps of 1 cm/s, a V-shaped flame could be sustained for values of U_{IN} as low as 8 cm/s (i.e., over a range where ignition/extinction flames are observed), showing that

there is a hysteresis in the transition between these two flame types.

3.2.3. Asymmetric stable flame ($77 \leqslant U_{IN} \leqslant 77.2$ cm/s)

An increase of the inlet velocity from 75.5 to 77 cm/s alters the entire flame structure. The flame is no longer symmetric with respect to the midplane; moreover, two steady asymmetric flames can be obtained for the same value of U_{IN}. The flames form an obtuse or an acute angle with the lower wall and will be referred to as *lower* and *upper asymmetric*, respectively. Figs. 7a, 7e, to be discussed in detail within the context of Section 3.2.5, show the Y_{OH} distribution of such flames for $U_{IN} = 77$ cm/s. Over the narrow range of coexistence of these two flames ($77 < U_{IN} < 77.2$ cm/s), transitions between them can be induced by appropriately perturbing the flames. From the dynamical system point of view, the transition from a V-shaped symmetric to an asymmetric flame results from a symmetry-breaking pitchfork bifurca-
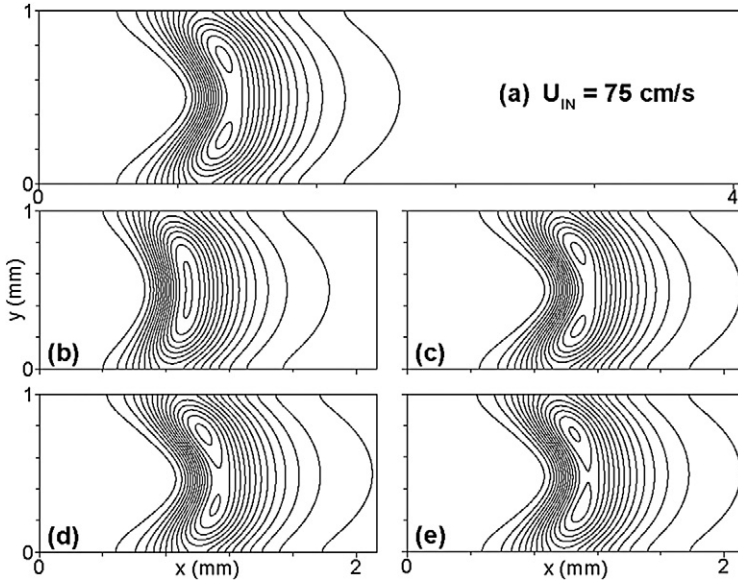
Fig. 4. Isolines of H mass fraction in the $h = 1.0$ mm height channel: (a) V-shaped steady flame with two Y_H maxima at $U_{IN} = 75$ cm/s; (b) to (e) during the transient after an impulsive change of the inflow velocity from $U_{IN} = 60$ cm/s (V-shaped flame) to 77.2 cm/s (asymmetric flame) at $t = 0.0$, 8.1, 19.4, and 30.5 ms, respectively. Fifteen isolines ranging from 5×10^{-6} to 1.715×10^{-4}, 1.51×10^{-4}, 1.74×10^{-4}, 1.82×10^{-4}, and 1.8×10^{-4} in (a)–(e), respectively, are plotted within the channel extent around the flame.

tion, where a real eigenvalue of the Jacobian of the conservation equations, linearized around the symmetric solution, crosses the imaginary axis through zero. It seems that the appearance of the two Y_H maxima triggers the asymmetry. This flame type does not persist for a wide range of U_{IN}, but reappears for higher values of the inflow velocity and is discussed in more detail in Section 3.2.5.

Figs. 4b–4e provide isolines of Y_H at four time instants during the transient after an impulsive change of U_{IN} from 60 to 77.2 cm/s, leading from a V-shaped flame with a single Y_H maximum to an asymmetric flame. It can be clearly seen that the two symmetric in location and value Y_H maxima appear first (Fig. 4c). However, this structure is no longer stable and finally evolves into the asymmetric flame of Fig. 4e.

Close examination of the transition from the V-shaped to the asymmetric flame reveals that the transition occurs via damped oscillations with a characteristic frequency. This indicates that two modes of the stable V-shaped flame are responsible for the observed behavior. The first one is associated with the transition to the asymmetric flame and becomes unstable (the corresponding real eigenvalue becomes positive) for a value of the inflow velocity in the range $77 < U_{IN} < 77.2$ cm/s. The second mode is associated with the damped oscillations, and is therefore stable in this inflow velocity range.

3.2.4. Oscillating flame ($77.5 \leqslant U_{IN} \leqslant 113$ cm/s)

Starting from the steady asymmetric flame at $U_{IN} = 77.2$ cm/s, the increase to $U_{IN} = 77.5$ cm/s results in a self-sustained oscillation with the flame shape changing periodically between the upper and the lower asymmetric structure. This behavior, while it appears like a regular limit cycle, actually connects the two asymmetric solutions, and can therefore be attributed to a global bifurcation (heteroclinic connection).

For $U_{IN} = 84$ cm/s, the value of the maximum temperature oscillates between 1418 and 1482 K, with a frequency of 490 Hz (Fig. 5a). The period of the temperature oscillation plotted in Fig. 5a is the time needed for a change of the flame from the upper (Fig. 5b) to the lower asymmetric shape (Fig. 5e) or vice versa; therefore, it is half the period of the full flame oscillation. The maxima of all species mass fractions and temperature shift periodically between two positions located above and below the midplane, and the flame shape changes smoothly between a lower asymmetric (Fig. 5b) and an upper asymmetric flame (Fig. 5e). This behavior persists for the inflow velocity range $77.5 \leqslant U_{IN} \leqslant 113$ cm/s. The increase in the frequency and amplitude, $\Delta T = T_{max} - T_{min}$, of the oscillations with increasing U_{IN} is illustrated in Fig. 6.
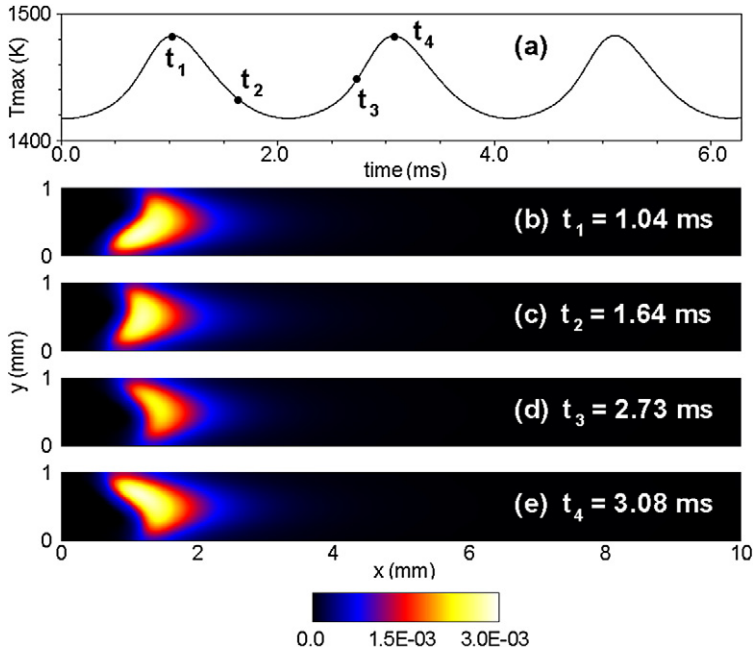
Fig. 5. Oscillating flame for $U_{IN} = 84$ cm/s in the $h = 1.0$ mm channel; (a) temporal variation of the maximum flame temperature; (b) to (e) provide the OH mass fraction at the four times t_1 to t_4 of the oscillation period marked in (a).
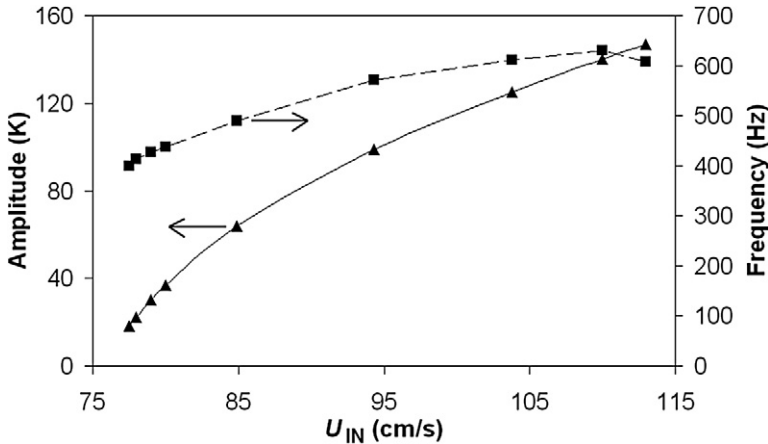

Fig. 6. Influence of the inflow velocity U_{IN} on the maximum temperature oscillation amplitude and frequency for the $h = 1.0$ mm channel.

3.2.5. Asymmetric stable flames ($109 \leqslant U_{IN} \leqslant 400$ cm/s)

By increasing the inflow velocity from 113 to 117 cm/s the oscillations cease, the flame becomes steady, and it further assumes an asymmetric shape. The distribution of the OH mass fraction for the two stable flame structures that coexist for the rest of the investigated inflow velocities is shown in Fig. 7 for $U_{IN} = 165$, 300, and 400 cm/s. The upper or lower asymmetric flames can be obtained either by starting from a suitable initial condition, or by appropriately perturbing the system. For example, an increase of the

maximum temperature of one wall by 6 K is sufficient to force the transition from one asymmetric flame to the other. The attained asymmetric flame remains stable when the wall temperatures are subsequently reset equal to each other. As U_{IN} increases, the flame stabilizes farther downstream and it is, eventually, blown out for high enough inflow velocity.

Starting from the asymmetric flame at $U_{IN} = 113$ cm/s and gradually reducing the inflow velocity in steps of 1 cm/s, the asymmetric flame remains stable up to $U_{IN} = 109$ cm/s. Therefore, for $109 \leqslant U_{IN} \leqslant 113$ cm/s, oscillating and asymmetric flames
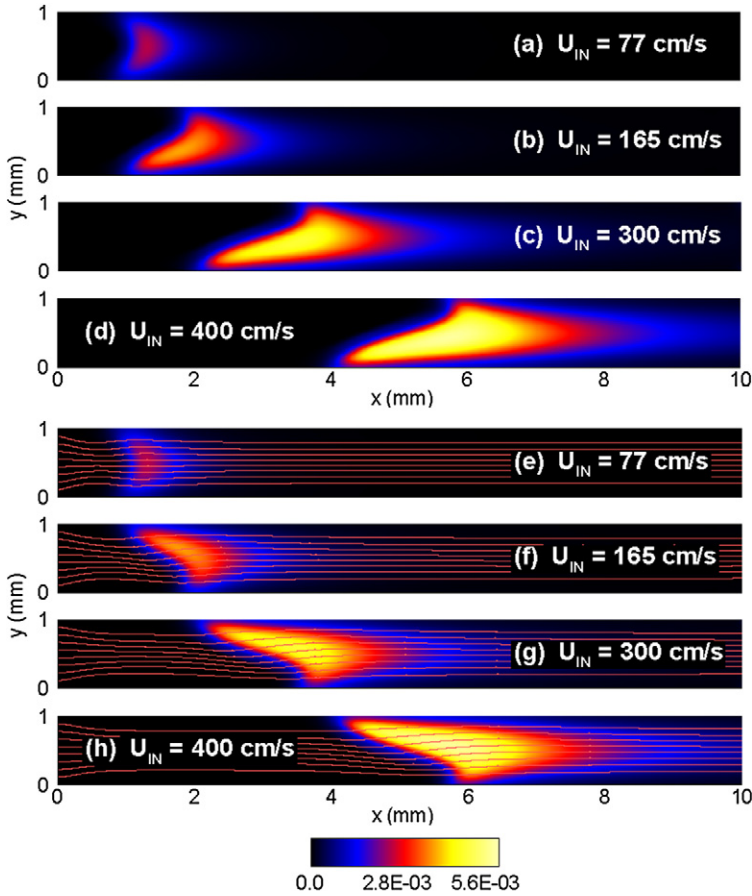
Fig. 7. Asymmetric type flames in the $h = 1.0$ mm height channel, (a, b, c, d) upper and (e, f, g, h) lower asymmetric flames: OH radical mass fraction for different values of the inflow velocity U_{IN} ($U_{IN} = 165$ cm/s, $U_{IN} = 300$ cm/s, $U_{IN} = 400$ cm/s). In (e, f, g, h) the flow streamlines are superimposed.

coexist and the transition between them is associated with hysteresis.

Asymmetric stable flames of the type reported in Fig. 7 have also been observed experimentally in Dogwiler et al. [34] for $\varphi = 0.33$ CH$_4$/air mixtures in a planar channel-flow configuration established between two plates 250 mm long, 110 mm wide, and placed 7 mm apart. Therein, at random time intervals (triggered by small experimental parameter variations) the flame changed from upper asymmetric to lower asymmetric and vice versa. In other theoretical and numerical works the stability of axisymmetric flames in cylindrical tubes has led to contradicting results: Metzener and Matalon [33] in their numerical simulations reported the existence of a critical tube diameter above which only axisymmetric flames are stable. On the other hand, Petchenko and Bychkov [35] showed by means of linear stability analysis that the axisymmetric flame is unstable at any tube radius; instead flames with nonaxisymmetric structure have to be expected.

3.2.6. Summary of flame dynamics in the 1.0-mm-height channel

To distinguish the different types of flames and to have a unique and coherent indicator for the flame dynamics, it is useful to define a new parameter, h_{max}. It represents the transverse distance from the lower plate ($y/h = 0.0$) of the farthest from the inflow point on the $Y_{H_2} = 0.007$ isolevel of the mass fraction of molecular hydrogen, nondimensionalized by the channel height (the chosen value of Y_{H_2} is half of the maximum, but the particular choice does not affect the results in any way). Thus, for a V-shaped stable flame, the flame tip is located at the channel midplane and $h_{max} = 0.5$. For the upper (Figs. 7a–7d) and lower (Figs. 7e–7h) asymmetric flames, the maximum flame penetration (flame tip) is closer to the upper (lower) wall, so that $h_{max} > 0.5$ ($h_{max} < 0.5$).

The complete description of the flame dynamics in the 1.0 mm channel is summarized in Fig. 8, depicting all the transitions from the repetitive ignition/extinction at the lowest inflow velocities (marked
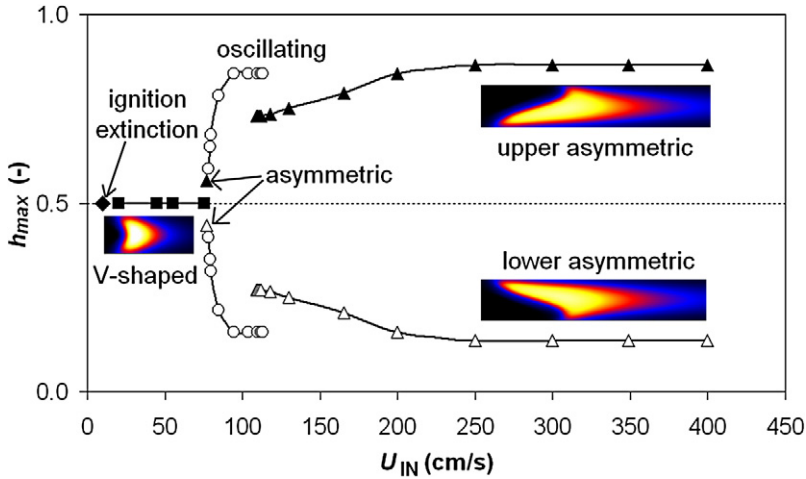
Fig. 8. Flame stability diagram for the $h = 1.0$ mm height channel. The images show the OH radical mass fraction. For clarity, the following computed points are not reported in the diagram: $U_{IN} = 4, 7, 13, 15, 16, 17, 18, 19, 30, 50, 60, 77.2, 77.5$ cm/s (the dotted line does not represent any solution).
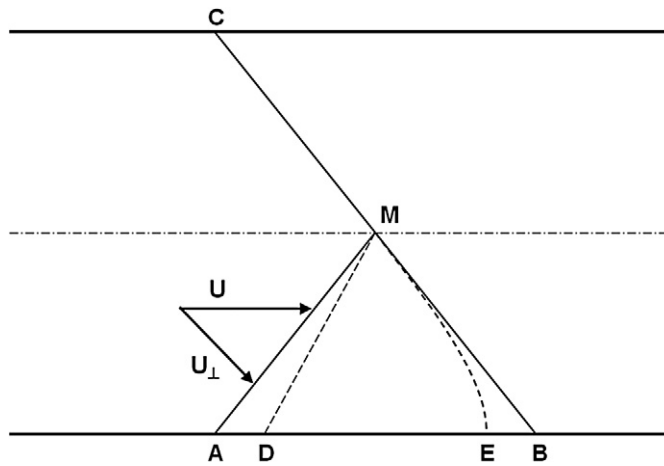

Fig. 9. Schematic explaining the instability leading from a V-shaped to an asymmetric flame.

with filled rhomboids), to the stable V-shaped symmetric flames (filled squares), to the steady asymmetric flame (filled and open triangles for the upper and lower asymmetric flames, respectively), to the oscillating flames (open circles), and finally again to the steady asymmetric flames, which eventually blow out for high enough inflow velocities.

In Fig. 9, it is attempted to show qualitatively that asymmetric flames can also be stable and, therefore, observable states. A V-shaped flame is denoted by A–M–C. On the two branches A–M and M–C the normal component of the incoming mixture velocity to the flame must be equal to the local burning velocity for the flame to be stabilized. Starting from this configuration, if one of the two branches is slightly perturbed, e.g., the branch A–M to D–M, the normal component $U_\perp$ increases and becomes larger than

the local burning velocity, so that the branch D–M is unstable and may move to the configuration B–M, which, using analogous considerations, can be shown to be stable. Because of the higher preheating of the mixture in this new configuration, the flame anchoring point is shifted slightly upstream, namely from B to E.

3.3. The 0.9-mm channel

Simulations have been performed at mixture inflow velocities U_{IN} varying from 10 cm/s ($Re_{IN} = 4.8$) to 400 cm/s ($Re_{IN} = 191$). The flame stability diagram, shown in Fig. 10, is qualitatively the same as the one for the 1.0 mm channel, i.e., periodic extinction and reignition ($U_{IN} = 10$ cm/s), symmetric V-shaped flames ($30 \leqslant U_{IN} \leqslant 93$ cm/s), displaying two Y_H maxima for $U_{IN} \geqslant 70$ cm/s,
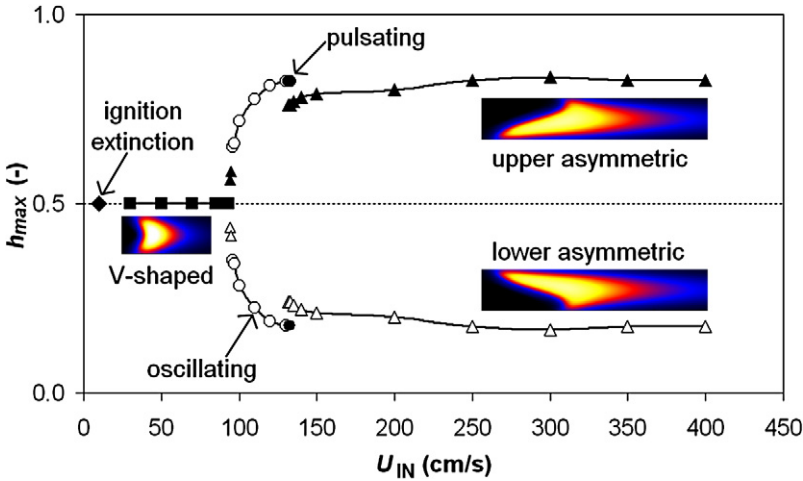
Fig. 10. Flame stability diagram for the $h = 0.9$ mm height channel. The images represent the OH radical mass fraction (the dotted line does not represent any solution).
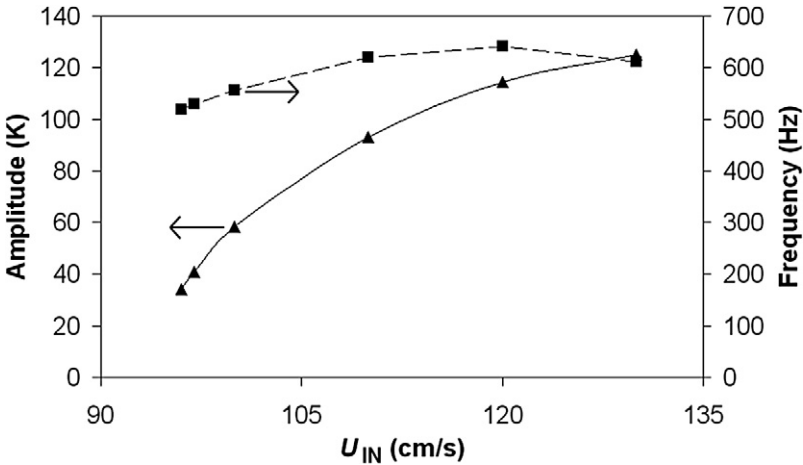

Fig. 11. The influence of the inflow velocity U_{IN} on the maximum temperature oscillation amplitude and frequency for the $h = 0.9$ mm channel.

asymmetric flames ($94 \leqslant U_{IN} \leqslant 95$ cm/s), oscillating ($96 \leqslant U_{IN} \leqslant 133$ cm/s), and again asymmetric flames ($U_{IN} > 132$ cm/s).

The amplitude and frequency for varying U_{IN} of the oscillating modes are shown in Fig. 11. These modes are of the same type as for the 1.0-mm channel, except for $U_{IN} = 132$ and 133 cm/s (not shown in Fig. 11). For $U_{IN} = 133$ cm/s, the mode of oscillations changes completely: the flame maintains a constant shape (one of the two asymmetric structures) and oscillates along the flow direction. We will call this streamwise oscillating flame *pulsating* to distinguish it from the flame that oscillates between the two asymmetric shapes. The streamwise position of the maximum Y_H, $x(Y_{H,max})$, of this flame changes between the values 1.15 and 1.75 mm with a frequency of 631 Hz; the amplitude of the associated maxi-

mum temperature oscillation is 114 K. For $U_{IN} = 132$ cm/s, the flame exhibits an oscillatory behavior that is a hybrid between the oscillating and the pulsating flame. In addition to periodically changing between the upper to the lower asymmetric structures (oscillating flame), during certain time intervals, it assumes one of the asymmetric shapes and oscillates weakly along the flow direction (pulsating flame).

3.4. The 0.8-mm channel

The same range of inflow velocities was considered ($10 \leqslant U_{IN} \leqslant 400$ cm/s, corresponding to $4.2 \leqslant Re_{IN} \leqslant 170$). The observed dynamics are qualitatively similar to those of the 0.9 mm channel and are summarized in Fig. 12a. For the lower inlet velocity range, $10 \leqslant U_{IN} \leqslant 20$ cm/s, ignition/extinction
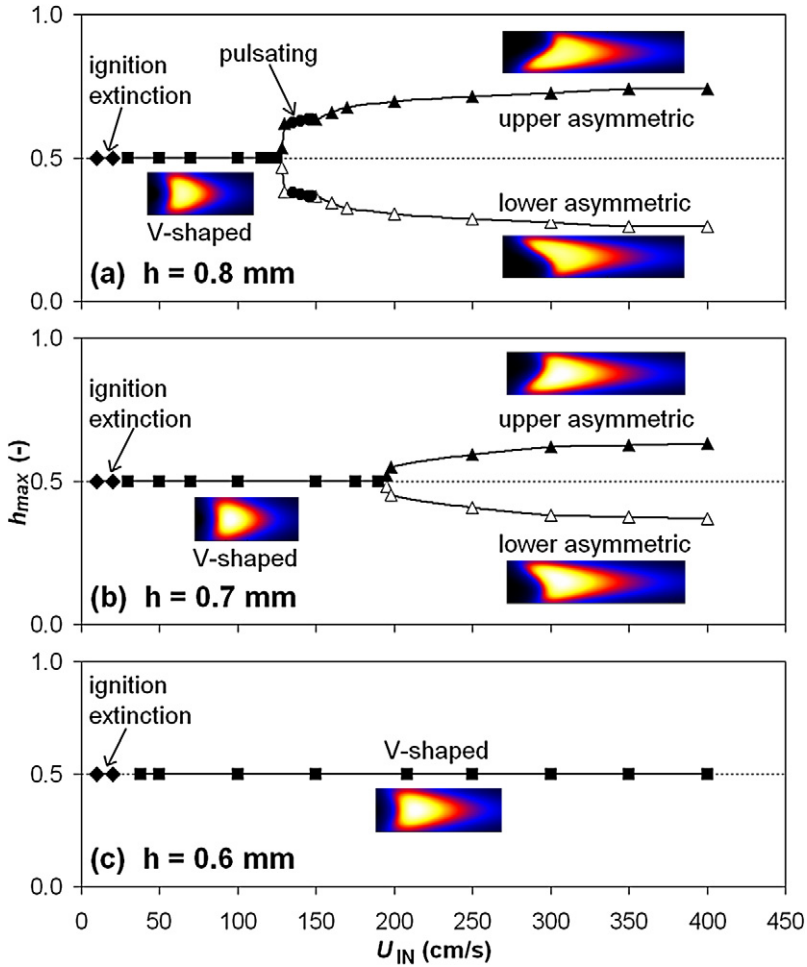
Fig. 12. Flame stability diagram for the (a) $h = 0.8$ mm, (b) $h = 0.7$ mm, and (c) $h = 0.6$ mm channels. The images represent the OH radical mass fraction (the dotted lines do not represent any solution).
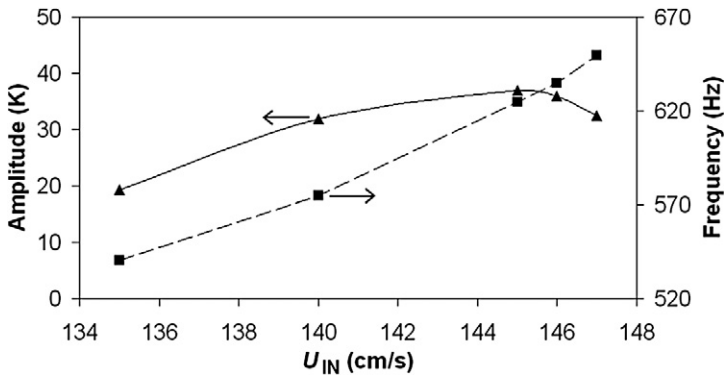

Fig. 13. The influence of the inflow velocity U_{IN} on the maximum temperature oscillation amplitude and frequency for the $h = 0.8$ mm channel.

phenomena are observed, as further discussed in the forthcoming Fig. 16. V-shaped flames are obtained for inflow velocities in the range $30 \leqslant U_{IN} \leqslant 125$ cm/s.

Once again, two maxima of the H mass fraction appear for $U_{IN} > 115$ cm/s. Increasing the velocity from $U_{IN} = 125$ to 128 cm/s, the flame changes from
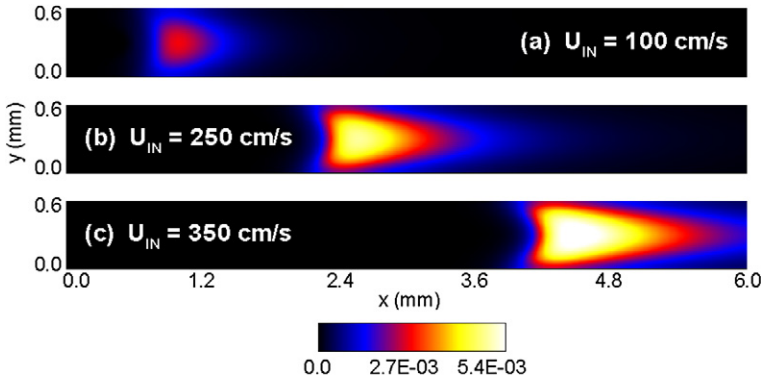
Fig. 14. V-shaped flames for the $h = 0.6$ mm channel; OH radical mass fraction maps for increasing values (from top to bottom) of the inflow velocity (a) $U_{IN} = 100$ cm/s, (b) $U_{IN} = 250$ cm/s, and (c) $U_{IN} = 350$ cm/s.
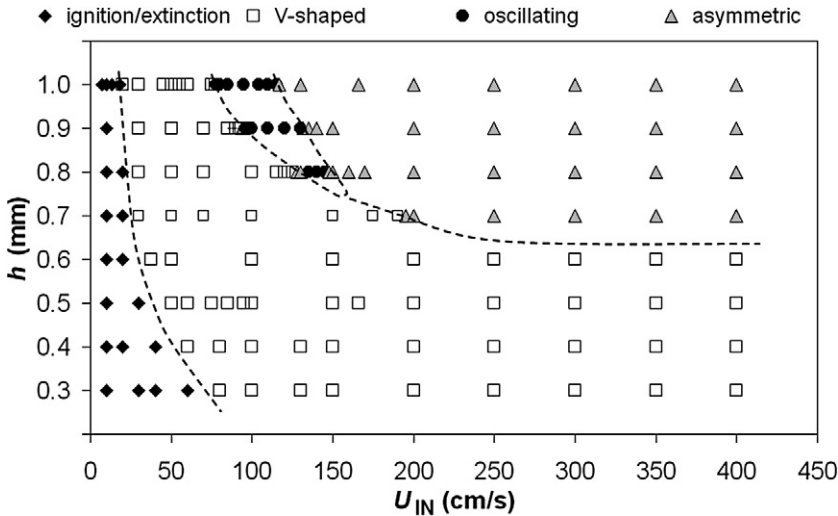

Fig. 15. Global stability diagram. For clarity, the lines showing the hysteresis in the transition from the ignition/extinction to the V-shaped flame in the $h = 1.0$ mm channel, the narrow range of asymmetric flames established between the V-shaped and the oscillating flames, the hysteresis in the transition from oscillating to asymmetric, and finally the pulsating flames which are included in the oscillating ones have been omitted.

V-shaped to steady asymmetric, which remains stable up to $U_{IN} = 130$ cm/s. The oscillatory flames observed over the narrow range $135 \leqslant U_{IN} \leqslant 147$ cm/s display only the pulsating mode of oscillation (back and forth in the streamwise direction, while remaining asymmetric). They result from a supercritical Hopf bifurcation of the asymmetric flames. Fig. 13 provides the amplitude and frequency of the pulsations. Increasing U_{IN} from 147 to 150 cm/s results in slow dampening of the pulsations, until, past a second Hopf, the flame stabilizes in one of the asymmetric positions. From there on, an increase of the inlet velocity does not produce any change in the flame configuration, except that the asymmetric flame is pushed toward the outflow for higher U_{IN}.

3.5. The 0.7-mm channel

Simulations have been performed for inflow velocities varying from 10 cm/s ($Re_{IN} = 3.7$) to 400 cm/s ($Re_{IN} = 148$). The sequence of transitions for this case are periodic ignition/extinction ($10 \leqslant U_{IN} \leqslant 20$ cm/s), symmetric V-shaped flame ($30 \leqslant U_{IN} \leqslant 190$ cm/s), V-shaped flame with two maxima of the Y_H ($U_{IN} = 193$ cm/s), and asymmetric flames ($195 \leqslant U_{IN} \leqslant 400$ cm/s) as seen in Fig. 12b. Increasing the inlet velocity from 193 to 195 cm/s changes the V-shaped flame to an asymmetric one; this flame structure remains stable upon further increase of U_{IN}, stabilizing further away toward the outflow (see also Fig. 17b). It is evident that the range of inlet velocities, wherein a V-shaped
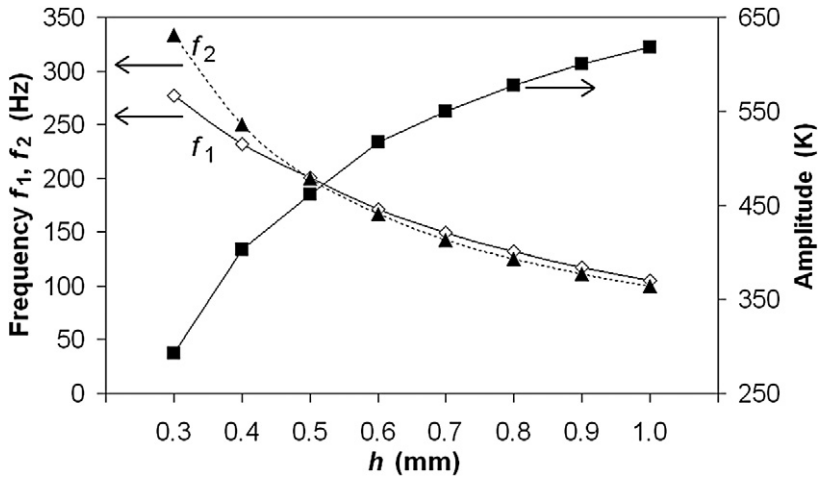
Fig. 16. Frequency (f_1) and amplitude ($T_{max} - T_W$) of the ignition/extinction combustion mode at $U_{IN} = 10$ cm/s for varying channel height. The frequency f_2 is the ratio between the inlet velocity U_{IN} and the channel height.

stable flame can be established, diminishes with increasing channel height h (see Figs. 8, 10, and 12).

3.6. The 0.6-mm to 0.3-mm channels

The asymmetric flames vanish for channel heights equal to or less than 0.6 mm, and the only flame structures observed are of the periodic ignition/extinction and V-shaped types. We have even tried to force the jump to the asymmetric branch by imposing an asymmetric flame as initial condition, but in very short time the flame assumed the symmetric shape. The much simpler stability diagram for the 0.6 mm channel is shown in Fig. 12c. In narrower channels the only difference is the value of U_{IN} for the transition from ignition/extinction to V-shaped (about 40, 50, and 70 cm/s for $h = 0.5$, 0.4, and 0.3 mm, respectively) and also the frequency and amplitude of the ignition/extinction oscillations. By increasing the inflow velocity, the V-shaped flame moves toward the outflow, and is almost blown out for the highest velocities considered; see Figs. 14 and 17a.

4. Summary of combustion dynamics

The results are summarized in the two-parameter diagram of Fig. 15; for clarity, the pulsating and the oscillating flame types and the regions of coexistence of different flame types are not distinguished. As already mentioned, increasing the channel height from 0.3 to 1.0 mm leads to richer dynamics. In narrow channels only symmetric stable V-shaped flames are formed (the ignition/extinction mode is always present). Asymmetric flames can no longer be stabilized when the channel height is smaller than roughly

twice the laminar flame thickness. It is also worth pointing out that, in all cases, the transitions from the V-shaped to the asymmetric flames are preceded by the appearance of the two maxima in the profiles of the H mass fractions.

For all the channel heights considered, there is an ignition/extinction regime at the lowest velocity range. Fig. 16 summarizes the frequency f_1 and amplitude ($T_{max} - T_W$) of this combustion mode at $U_{IN} = 10$ cm/s as functions of the channel height. Increasing h from 0.3 to 1.0 mm results in an amplification of the amplitude from about 300 up to 618 K and in a drop of the frequency from 277 to 105 Hz. In the same figure, the characteristic frequency $f_2 = U_{IN}/h$ corresponding to the channel height and to the inflow velocity is also reported; it has almost the same value as the ignition/extinction frequency, particularly for $h \geqslant 0.5$ mm, resulting in a Strouhal number St $= f_1 \times h/U_{IN} \approx 1.0$. The frequency increase of the ignition/extinction mode with decreasing tube diameter was also observed experimentally by Richecoeur and Kyritsis [6]. It can be explained by considering that as the channel height decreases, the time needed to heat up the fresh inflowing mixture until it ignites becomes shorter; therefore, the distance of the ignition location from the inlet section is shorter, and the frequency of the process increases.

Figs. 17a and 17b provide the nondimensional streamwise flame location inside the channel for $0.3 \leqslant h \leqslant 0.6$ mm and $0.7 \leqslant h \leqslant 1.0$ mm, respectively. The flame location is identified as the streamwise position of the maximum H radical mass fraction, $x(Y_{H,max})$, nondimensionalized with the channel height h. Only the location of the V-shaped and asymmetric type flames is shown, since the ignition/extinction and oscillating flames are not steady.
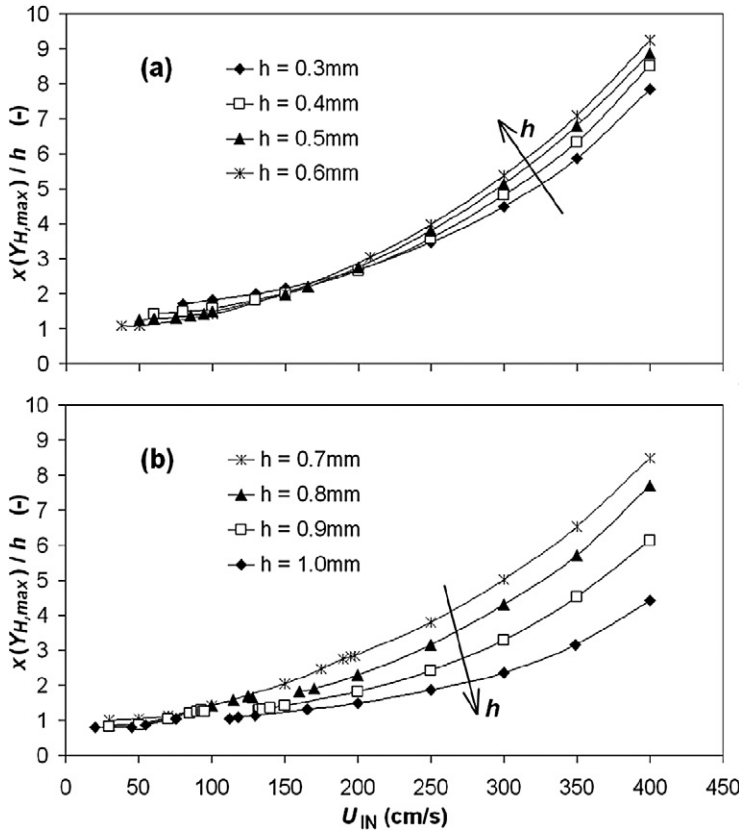
Fig. 17. Nondimensional flame penetration as a function of U_{IN}: (a) channel heights 0.3, 0.4, 0.5, and 0.6 mm; (b) channel heights 0.7, 0.8, 0.9, and 1.0 mm.

By increasing the inlet velocity, the flame is convected downstream. As the channel height increases from 0.3 to 0.6 mm (Fig. 17a), the time scale for heat transfer from the reaction zone to the walls and from the hot walls to the incoming reactants increases. As a result, the flame stabilizes farther downstream. For inlet velocities less than 150 cm/s, this behavior is inversed. The situation is different for channel heights between 0.7 and 1.0 mm (Fig. 17b); increasing the channel height always causes a significant decrease in flame streamwise penetration. However, it should be pointed out that the flames in the smaller channels ($h = 0.3$ to 0.6 mm) are V-shaped, while those of wider ones ($h = 0.7$ to 1.0 mm) are V-shaped and asymmetric for low and high U_{IN}, respectively.

Fig. 18 illustrates the maximum temperature of the steady (V-shaped and asymmetric) flames inside the channel for different values of the inlet velocity and for all the simulated channel heights. In some cases, namely channels with $0.7 \leqslant h \leqslant 1.0$ mm and for high inlet velocities, the maximum temperature inside the channel is slightly higher than the adiabatic flame temperature ($T_f = 1630$ K), whereas in all other cases it is consistently lower. This is related to a tradeoff be-

tween the preheating of the fresh mixture before the reaction zone by the channel hot walls ($T_W > T_{IN}$) and the heat loss from the flame zone to the channel walls ($T_{flame} > T_W$). If U_{IN} is low, the streamwise position of the flame inside the channel is such that the heat loss to the walls from the flame zone dominates over the mixture preheat.

The frequency of the oscillatory flames in the 0.8-, 0.9-, and 1.0-mm channels depends on channel height and inlet velocity and varies between 100 and 600 Hz, while the oscillation amplitude can reach values as large as 140 K.

4.1. Effect of reaction mechanism

In order to asses the dependence of the observed dynamics on the particular choice of the reaction mechanism, simulations with the detailed H_2/air mechanism of Warnatz et al. [36] were also performed. The comparison was done for the 1.0-mm-height channel for (a) an oscillating flame at $U_{IN} = 104$ cm/s and (b) an upper asymmetric one at $U_{IN} = 165$ cm/s; both flames were reproduced by the Warnatz scheme. The oscillating flame computed
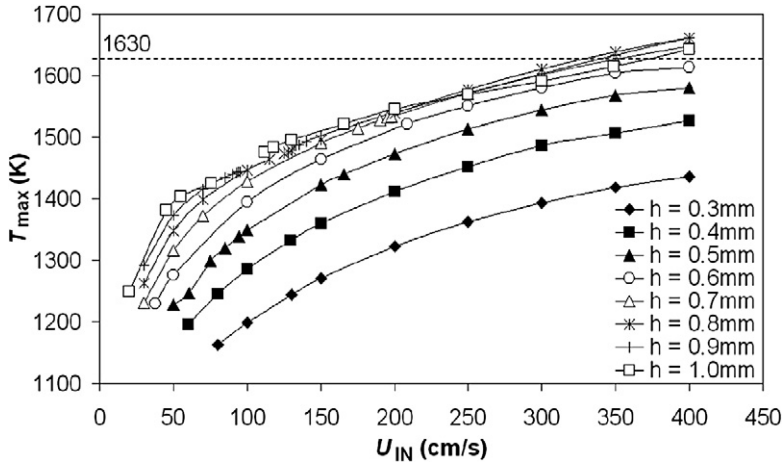
Fig. 18. Maximum temperature inside the channel as a function of the inlet velocity U_{IN}.

with the latter mechanism reveals a slight downstream displacement of the flame coupled with the oscillating mode. The oscillation frequency is 467 Hz and the amplitude 158 K (the corresponding values for the Yetter mechanism are 611 Hz and 125 K). The upper asymmetric flame computed with the Warnatz mechanism is located 1.79 mm downstream of the inlet, while the one computed with the Yetter mechanism 1.30 mm.

4.2. Effect of Lewis number

The influence of Lewis number on the flame dynamics has been analyzed for the 1.0-mm channel height by setting the molecular diffusivity of all species equal to the mixture thermal diffusivity. While the critical values of U_{IN} for the transitions between the different flame types were different, the stability diagram for the unity Lewis number flames remained qualitatively the same as in Fig. 8. However, because of the presence of heat losses, which have a strong influence on the effective Lewis number [16], it cannot be concluded that the observed phenomena are not related to a thermodiffusive instability.

4.3. Effect of inflow velocity profile

The particular choice of the inflow velocity profile is expected to have a strong effect on the flame behavior, especially in cases where the flame is located closed to the inflow. Two simulations were performed with parabolic inflow velocity profiles for $U_{IN} = 94$ and 250 cm/s, using as initial conditions the corresponding oscillating and asymmetric flame, respectively. The oscillating flame became steady and V-shaped, while the asymmetric one did not change in structure. Since the entire range of inflow velocities

has not been examined, it is not certain whether the U_{IN} range for which the oscillating flame exists is simply altered when changing the inflow velocity profile. Nonetheless, there is evidence that the richness of the observed dynamics will be reduced when the inflow profile is parabolic. It should be noted, however, that for practical systems the uniform inflow velocity profile is more realistic.

5. Conclusions

The dynamics of fuel-lean premixed hydrogen/air combustion in micro-scale plane channels were investigated by means of direct numerical simulation with detailed chemistry and transport. A two-parameter study has been performed, with respect to the channel height and the inflow velocity, which have been varied in the range of $0.3 \leqslant h \leqslant 1.0$ mm and $4 \leqslant U_{IN} \leqslant 400$ cm/s, respectively.

Five types of flames have been found for increasing inflow velocity at a fixed channel height. The richest behavior is observed for the wider channels: For low velocities, periodic ignition/extinction is observed that can be viewed as a connection between the burning and the cold solution. As U_{IN} is increased, there is a hysteretic transition to a V-shaped steady flame. A symmetry-breaking pitchfork bifurcation subsequently leads to two asymmetric flames. For channel heights larger than 0.8 mm, these flames undergo a global bifurcation to a structure oscillating between the two asymmetric flames. For lower channel heights, a different oscillatory mode, asymmetric flames pulsating axially, is obtained after a supercritical Hopf bifurcation. The asymmetric flames re-emerge at higher U_{IN} after the pulsating flames lose stability at a subcritical Hopf. The asymmetric flames are then convected downstream and eventu-

ally blow off at high enough inflow velocities. The observed dynamics are found to be insensitive to the specific chemical reaction mechanism and to transport properties (Lewis numbers).

The ignition/extinction, the oscillating, and the pulsating types lead to high-frequency periodic variations of the flame characteristics, such as temperature variations of hundreds of degrees. The oscillating, pulsating, and asymmetric flame types disappear when the channel height is reduced below a value which is roughly twice the laminar flame thickness. The ignition/extinction mode and the V-shaped flame are present for all channel heights considered. A global stability map, delineating the regions of the different flame types in the inlet velocity/channel height parameter space, is constructed.

We are currently investigating premixed flame dynamics in channels with heights larger than 1.0 mm. We also plan to investigate the effect of equivalence ratio and wall temperature on the observed dynamics.

Acknowledgments

References

[1] A.C. Fernandez-Pello, Proc. Combust. Inst. 29 (2002) 883–899.

[2] A.R. Jones, S.A. Lloyd, F.J. Weinberg, Proc. R. Soc. London Ser. A 360 (1978) 97–115.

[3] C. Miesse, R.I. Masel, M. Short, M.A. Shannon, Combust. Theory Modelling 9 (2005) 77–92.

[4] K. Maruta, J.K. Parc, K.C. Oh, T. Fujimori, S.S. Minaev, R.V. Fursenko, Combust. Explos. Shock Waves 40 (2004) 516–523.

[5] K. Maruta, T. Kataoka, N.I. Kim, S. Minaev, R. Fursenko, Proc. Combust. Inst. 30 (2005) 2429–2436.

[6] F. Richecoeur, D.C. Kyritsis, Proc. Combust. Inst. 30 (2005) 2419–2427.

[7] L. Landau, Acta Physicochim. (URSS) 19 (1944) 77–85.

[8] G. Darrieus, Propagation d'un front de flame, in: Sixth International Congress of Applied Mathematics, 1946.

[9] V.V. Bychkov, M.A. Libermann, Phys. Rep. 325 (2000) 115–237.

[10] G.I. Barenblatt, Y.B. Zeldovich, A.G. Istratov, J. Appl. Mech. Tech. Phys. 4 (1962) 21–26.

[11] G. Joulin, P. Clavin, Combust. Flame 35 (1979) 139–153.

[12] P.D. Roney, Combust. Flame 82 (1990) 1–14.

[13] C. Cui, M. Matalon, T.L. Jackson, AIAA J. 43 (2005) 1284–1292.

[14] E.W. Christiansen, C.K. Law, Proc. Combust. Inst. 29 (2002) 61–68.

[15] S. Ishizuka, K. Miyasaka, C.K. Law, Combust. Flame 45 (1982) 293.

[16] J.K. Bechtold, C. Cui, M. Matalon, Proc. Combust. Inst. 30 (2004) 177–184.

[17] J. Buckmaster, SIAM J. Appl. Math. 43 (1983) 1335.

[18] J. Daou, M. Matalon, Combust. Flame 124 (2001) 337–349.

[19] T.L. Jackson, J. Buckmaster, Z. Lu, D.C. Kyritsis, L. Massa, Proc. Combust. Inst. 31 (2007) 955–962.

[20] S. Raimondeau, D. Norton, D.G. Vlachos, R.L. Masel, Proc. Combust. Inst. 29 (2002) 901–907.

[21] N. Kim, K. Maruta, Combust. Flame 146 (2006) 283–301.

[22] D.G. Norton, D.G. Vlachos, Chem. Eng. Sci. 58 (2003) 4871–4882.

[23] D.G. Norton, D.G. Vlachos, Combust. Flame 138 (2004) 97–108.

[24] S. Karagiannidis, J. Mantzaras, G. Jackson, K. Boulouchos, Proc. Combust. Inst. 31 (2007) 3309–3317.

[25] M.O. Deville, P.F. Fischer, E.H. Mund, High-Order Methods for Incompressible Fluid Flow, Cambridge University Press, New York, 2002.

[26] A.G. Tomboulides, J. Lee, S.A. Orszag, J. Sci. Comput. 12 (1997) 139–167.

[27] G.D. Byrne, A.C. Hindmarsh, Int. J. High Perform. Comput. Appl. 13 (1999) 354–365.

[28] R.A. Yetter, F.L. Dryer, H. Rabitz, Combust. Sci. Technol. 79 (1991) 97–128.

[29] R.J. Kee, G. Dixon-Lewis, J. Warnatz, M.E. Coltrin, J.A. Miller, A Fortran computer code package for the evaluation of gas-phase multicomponent transport properties, Report No. SAND86-8246, Sandia National Laboratories, 1996.

[30] R.J. Kee, F.M. Rupley, J.A. Miller, Chemkin II: A Fortran chemical kinetics package for the analysis of gas-phase chemical kinetics, Report No. SAND89-8009B, Sandia National Laboratories, 1996.

[31] T. Poinsot, D. Veynante, Theoretical and Numerical Combustion, Edwards, Philadelphia, 2005.

[32] F.M. Rupley, R.J. Kee, J.A. Miller, Premix: A Fortran program for modeling steady laminar one-dimensional premixed flames, Report No. SAND85-8240, Sandia National Laboratories, 1995.

[33] P. Metzener, M. Matalon, Combust. Theory Modelling 5 (2001) 463–483.

[34] U. Dogwiler, J. Mantzaras, P. Benz, B. Kaeppeli, R. Bombach, A. Arnold, Proc. Combust. Inst. 27 (1998) 2275–2282.

[35] A. Petchenko, V. Bychkov, Combust. Flame 136 (2004) 429–439.

[36] J. Warnatz, R.W. Dibble, U. Maas, Combustion, Physical and Chemical Fundamentals, Modeling and Simulation, Springer, New York, 1996.